

# Time-dependent density functional theory for quantum transport

Yanho Kwok, Yu Zhang, and GuanHua Chen\*  
*Department of Chemistry, The University of Hong Kong*  
(Dated: March 22, 2013)

Throughout the last few decades, the rapid miniaturization of electronic devices motivates lots of researches in quantum transport through molecular devices. In particular, the investigation of time-dependent transport through realistic system from first-principles is an important research aspect in quantum transport. In this paper, we will review the recent progress in the development of time-dependent density functional theory for quantum transport, discussing about its theoretical foundation as well as the computational aspect. In particular, the reduced-single electron matrix based hierarchical equation of motion approach, which is originated from the Liouville-von Neumann equation, will be reviewed in more details. The numerical implementation details will be discussed and simulation results of realistic molecular devices will be given.

PACS numbers: 71.15.Mb, 72.10.Bg, 73.23.Ad, 73.63.-b

## CONTENTS

I. Introduction	1	And great progress has been achieved throughout the last decades. <sup>4-12</sup>
II. Modeling the problem and NEGF formalism	2	On the experimental side, the advance in nanofabrication techniques allows the realization of molecular junction such that current through single molecules can be measured. And recent advancement has been made in measuring the transient current of quantum dots. <sup>13</sup>
III. Time dependent density functional theory	3	On the theoretical side, the Landauer-Büttiker formalism has become a standard and routine approach to study the steady state current through the molecular devices. Combined with effective single particle theory such as density functional theory (DFT) and Keldysh's non equilibrium Green's function (NEGF) formalism, <b>namely DFT-NEGF method</b> , we can carry out first principle simulation of molecular devices composed of hundreds of atoms readily to study their steady state properties. <sup>14,15</sup>
IV. TDDFT-NEGF formalism	4	If larger scale simulation is desirable, one can turn to empirical method such as tight binding method or density-functional tight-binding (DFTB) method, <sup>16,17</sup> which is a tight binding method parameterized with DFT calculation. If we would like to simulate even larger systems or include the effect of surrounding substrate into simulation, we can apply multi-scale quantum mechanics and electromagnetics (QM/EM) simulation. <sup>18,19</sup> In this case, QM method is applied for the molecular device region in which quantum effect is critical and classical EM method is used to describe the surrounding less important environment.
V. Reduced single electron density matrix based hierarchical equation of motion approach	5	
A. Numerical implementation	6	
B. Tight-binding model simulation	6	
VI. Wide Band Limit Approximation	7	
A. RSDM based HEOM in WBL approximation	7	
B. TDDFT(B)-NEGF-HEOM-WBL formalism	8	
C. First principle simulation results	8	
VII. Concluding remarks	9	
Acknowledgments	10	
References	10	

## I. INTRODUCTION

Given the rapid miniaturization of electronic devices<sup>1</sup> down to nanometer scale, whether it is possible to construct electronic devices from individual molecules becomes a natural and important question. Molecular electronics, which either refer to molecular materials for electronics in the top-down approach or electronics constructed with single molecules in the bottom-up approach,<sup>2</sup> have become an active research area in both fundamental science as well as technological application point of view. The idea of building electronics with single molecule is not new and can be dated back to the 1970s.<sup>3</sup>

This review, however, will focus on simulation of time-domain quantum transport phenomena of molecular devices,<sup>20-29</sup> in contrast to the energy domain steady state simulation mentioned above. Currently, time domain simulation is still a difficult and challenging area needed to be explored. Time domain simulation is of interest for a couple of reasons.<sup>30</sup> First, it allows us to follow the real time evolution of the system of interest under a time dependent bias voltage. We can then study the transient dynamics of the system, determine the switch-on time for devices and study how the current develops through the molecules after the voltage is turned on. We can also use it to study the AC response

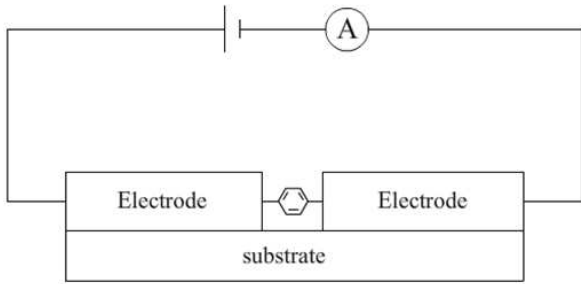


FIG. 1. Schematic diagram showing the experimental set-up for measuring current through molecular devices.

as well as response under any kinds of signal voltages since time-dependent simulation includes full frequency information.<sup>31</sup> Last but not least, the achievement of steady state is not guaranteed.<sup>32–35</sup> It has been shown that the presence of multiple bound states in the system can lead to a non-decaying oscillating current, which amplitude depends on the entire history of the applied voltage and can be larger than the steady state current.<sup>33,34</sup>

This review is organized as follows: first of all, we will give a brief introduction on how we model the quantum transport problem as well as the NEGF formalism. Second, we will talk about combining TDDFT and NEGF and the theoretical bases behind this. Third, an exact time-dependent density functional theory for quantum transport as well as practical numerical schemes are reviewed. Finally, an efficient computational scheme based on the commonly used wide-band limit (WBL) approximation is presented and numerical implement are demonstrated.

## II. MODELING THE PROBLEM AND NEGF FORMALISM

The typical experimental set-up measuring current through molecular devices is shown in the following schematic diagram (Fig. 1).

Modeling this experimental set-up is a difficult multi-scale problem since we have a microscopic molecules connected macroscopic electrodes, wires and power source. The common approach to model it is to partition the entire system into device and leads regions, as shown in Fig. 2. The central device region contains the molecular device of interest contacted with few atomic layers of the electrodes. This is the region where scattering takes place and thus the region we are interested in. Connected to the device region are the left and right lead regions, which act as electron reservoirs. Before switching on the voltage, the entire system is in equilibrium, sharing the same temperature and chemical potential. The application of bias voltage then shifts the Hamiltonian and chemical potential in the leads, creates an electric field in the device region and results in current flowing from

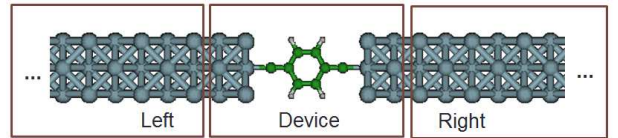


FIG. 2. Schematic diagram showing the partitioning of entire system into device and lead regions.

higher chemical potential side to lower side.

Now we come to the question how to treat the macroscopic leads properly. Early approaches ignore the lead region and simulate a finite system consisting of the device contacted with a few layers of the electrodes.<sup>36,37</sup> To prevent the back reflection from the lead boundary, complex absorbing potentials (CAP) can be applied at the edges of the finite leads to remove electrons reaching the edges.<sup>38,39</sup> Another approach is the Landauer-Büttiker approach. In this approach, we assume the electrodes extend semi-infinitely in the transport direction. With the Keldysh NEGF Formalism, we can treat the effect of the semi-infinite electrodes properly. Here we will give a brief review on it. Readers who are not familiar with the Keldysh NEGF Formalism are referred to Ref. 12 for more details.

Suppose our system is real space discretized or expanded by some orthonormal localized basis. Our system Hamiltonian can then be arranged and partitioned into the following form:

$$H = \begin{bmatrix} H_{LL} & H_{LD} & 0 \\ H_{DL} & H_{DD} & H_{DR} \\ 0 & H_{RD} & H_{RR} \end{bmatrix}, \quad (1)$$

where the diagonal block matrices  $H_{LL}, H_{DD}, H_{RR}$  are the Hamiltonian projected onto the left lead, central device and right lead regions respectively. The off-diagonal hopping matrices  $H_{LD} = H_{DL}^\dagger, H_{RD} = H_{DR}^\dagger$  represent the coupling between leads and device region. The retarded Green's function is then defined as:

$$\left[ i \frac{\partial}{\partial t} - H(t) \right] G^r(t, t') = \delta(t - t'), \quad (2)$$

which can be partitioned similarly as:

$$G^r = \begin{bmatrix} G^r_{LL} & G^r_{LD} & G^r_{LR} \\ G^r_{DL} & G^r_{DD} & G^r_{DR} \\ G^r_{RL} & G^r_{RD} & G^r_{RR} \end{bmatrix}. \quad (3)$$

Next, we define the bare Green's function  $g^r(t, t')$  for isolated regions as:

$$\left( i \frac{\partial}{\partial t} - H_{ii} \right) g^r_i(t, t') = \delta(t - t'), \quad (4)$$

where  $i = L, D, R$ . With the coupling between device and leads treated as perturbation, we apply Dyson's equation

$\mathbf{G}(t, t') = \mathbf{g}(t, t') + \int_{-\infty}^{\infty} d\tau \mathbf{g}(t, \tau) \mathbf{V}(\tau) \mathbf{G}(\tau, t')$  where

$$V = \begin{bmatrix} 0 & H_{LD} & 0 \\ H_{DL} & 0 & H_{DR} \\ 0 & H_{RD} & 0 \end{bmatrix}. \quad (5)$$

And obtain the Dyson equation for device retarded Green's function.

$$\begin{aligned} \mathbf{G}_{DD}^r(t, t') &= \mathbf{g}_{DD}^r(t, t') \\ &+ \sum_{\alpha=L,R} \int_{-\infty}^{\infty} d\tau_1 d\tau_2 \mathbf{g}_{DD}^r(t, \tau_1) \Sigma_{\alpha}^r(\tau_1, \tau_2) \mathbf{G}_D^r(\tau_2, t'), \end{aligned} \quad (6)$$

$$\mathbf{G}_{DD}^a(t, t') = \mathbf{g}_{DD}^a(t, t') + \sum_{\alpha=L,R} \int_{-\infty}^{\infty} d\tau_1 d\tau_2 \mathbf{g}_{DD}^a(t, \tau_1) \Sigma_{\alpha}^a(\tau_1, \tau_2) \mathbf{G}_D^a(\tau_2, t'), \quad (7)$$

$$\begin{aligned} \mathbf{G}_{DD}^{>,<}(t, t') &= \mathbf{g}_{DD}^{>,<}(t, t') + \sum_{\alpha=L,R} \int_{-\infty}^{\infty} d\tau_1 d\tau_2 [\mathbf{g}_{DD}^r(t, \tau_1) \Sigma_{\alpha}^r(\tau_1, \tau_2) \mathbf{G}_D^{>,<}(\tau_2, t') \\ &+ \mathbf{g}_{DD}^{>,<}(t, \tau_1) \Sigma_{\alpha}^a(\tau_1, \tau_2) \mathbf{G}_D^a(\tau_2, t') + \mathbf{g}_{DD}^r(t, \tau_1) \Sigma_{\alpha}^{>,<}(\tau_1, \tau_2) \mathbf{G}_D^a(\tau_2, t')]. \end{aligned} \quad (8)$$

Differentiating the above Dyson equations gives the Kadanoff-Baym equations, the equations of motion of the device Green's functions.

$$\begin{aligned} \left[ i \frac{\partial}{\partial t} - H_D(t) \right] G_D^{r/a}(t, t') &= \delta(t - t') \\ &+ \int_{-\infty}^{\infty} d\tau \Sigma_{\alpha}^{r/a}(t, \tau) G_D^{r/a}(\tau, t') \\ \left[ i \frac{\partial}{\partial t} - H_D(t) \right] G_D^{>,<}(t, t') &= \int_{-\infty}^{\infty} d\tau [\Sigma_{\alpha}^r(t, \tau) G_D^{>,<}(\tau, t') \\ &+ \Sigma_{\alpha}^{>,<}(t, \tau) G_D^a(\tau, t')] \end{aligned} \quad (9)$$

The Kadanoff-Baym equations determine the real-time evolution of the device region we are interested in. However, the initial values of the Green's functions need to be determined from the Dyson equations.

### III. TIME DEPENDENT DENSITY FUNCTIONAL THEORY

As mentioned, atomistic first principles simulations of molecular devices are useful in interpreting experimental results as well as giving prediction. Density functional theory (DFT) or time-dependent density functional theory (TDDFT) is probably the most commonly used method given its good accuracy and relatively small computational cost.

The theoretical foundation for density functional theory lies in the Hohenberg-Kohn (HK) theorem<sup>40</sup> which states that the ground state electron-density function determines uniquely the external potential and thus all electronic properties of the system. Similarly, the TDDFT is

where  $\Sigma_{\alpha}^r(\tau_1, \tau_2) = h_{D\alpha} g_{\alpha\alpha}^r(\tau_1, \tau_2) h_{\alpha D}$  is the self-energy accounting for the coupling between device and lead  $\alpha$ . The real part of self-energy describes the energy level shifting while its imaginary part gives the level broadening, accounting for the finite life time of electrons entering and leaving the device region. With the Langreth Rules for analytic continuation, we can obtain the Dyson's equation for the device advanced, lesser and greater Green's function similarly:

based on Runge-Gross theorem which shows that time-dependent electron density  $\rho(t)$  determines the electronic properties of a time-dependent system.<sup>41</sup> Following the suggestion by Kohn and Sham, instead of the original many-body interacting system, we simulate a reference non-interacting system with a carefully chosen Hamiltonian such that it reproduces exactly the same electron density  $\rho(t)$  as the original system. From the correct electron density, we can then obtain all electronic properties of interest. The Kohn Sham reference system Hamiltonian is given by:

$$H(t) = \sum_{i=1}^N h(\vec{r}_i, t) = \sum_{i=1}^N \left[ -\frac{1}{2} \nabla_i^2 + v_{KS}(\vec{r}_i, t) \right] \quad (10)$$

where  $v_{KS}(\vec{r}, t) = v_{ext}(\vec{r}, t) + v_H(\vec{r}, t) + v_{xc}(\vec{r}, t)$  is the effective Kohn-Sham(KS) potential which comprises of external potential, mean field electron-electron repulsion as well as exchange-correlation (XC) potential. If we are provided with the exact XC functional, this reference system in principle will evolve in a way that produces the exact electron density.

However, It should be noted that while the above two theorems are applicable only for isolated or closed system, the device region we are talking about is indeed an open system since electrons can enter and leave the region. Extending DFT or TDDFT to open system then relies on the so called holographic electron density theorem (HEDT). In 2004, Fournais et al.<sup>42,43</sup> first proved the analyticity of any time-independent the electron density of any real physical systems made of atoms and molecules. The analyticity of electron density means that given a piece of electron density on a finite subspace, we can in

principle do analytical continuation to obtain the electron density on the entire system. Thus the finite piece of electron density in the device region determines the electronic properties of the entire system. It is known as the holographic electron density theorem (HEDT) which forms the foundation for DFT for open system.

And in 2007, Chen et al. extended the HEDT to time-dependent case.<sup>24</sup> They proved that if the initial (at  $t = t_0$ ) electron density  $\rho(r, t_0)$  as well as the time-dependent external potential  $v(r, t)$  are real analytic in r-space, then the electron density on any finite subsystem at any time  $\rho_D(r, t)$  determines uniquely the electron density of whole system. This means that in principle we can extract all electronic properties of the system from the electron density within the device region. This time-dependent holographic electron density theorem (TD-HEDT) proves the existence of TDDFT method for open system and provides a legitimate for us to combine TDDFT and NEGF formalism.<sup>24,44</sup> **If current density is employed as the basic physical quantity of interest, the extension of time-dependent current-density functional theory (TDCDFT)<sup>45</sup> to open quantum system was rigorously established, which was termed as stochastic TDCDFT.<sup>46,47</sup>**

In the TDDFT-NEGF formalism, we can solve the Dyson equation or the Kadanoff-Baym equations with the Kohn-Sham time-dependent Hamiltonian  $h(t) = -\frac{1}{2}\nabla^2 + v_{KS}(\vec{r}, t)$ . It is noted that within the TDDFT formalism, all many body effects are in principle included in the exchange-correlation potential in this single particle Hamiltonian which is local in both time and space.

#### IV. TDDFT-NEGF FORMALISM

The first computational scheme which combines TDDFT and NEGF to simulate transient response with the infinite leads set-up was suggested by Kurth et al.<sup>22</sup> Instead of the Kadanoff-Baym equations, they partition time-dependent Schrodinger equation into leads and device region and derive the Schrodinger equation for the projected wave function onto device region.

$$i\frac{\partial}{\partial t}\psi_D(t) = H_D(t)\psi_D(t) + i\sum_{\alpha} H_{D\alpha}g(t, t_0)\psi_{\alpha}(t_0) + \sum_{\alpha} \int_{t_0}^t dt' \Sigma_{\alpha}(t, t')\psi_D(t') \quad (11)$$

The second last term is called the source term describing the injection of electron from leads into the device region. The last term corresponds to the so called memory term since it involves a time integral of the past history from  $t_0$  to  $t$ . Practically, they integrate the time-dependent Schrodinger equation and replace the propagator  $\exp(-iH\Delta t)$  by a finite difference representation known as Cayley's form.

$$\exp(-iH\Delta t) = \frac{1 - i\frac{\Delta t}{2}H}{1 + i\frac{\Delta t}{2}H} + O(\Delta t^2) \quad (12)$$

A discretized version which propagates  $\psi_D$  from the  $m^{\text{th}}$  time step to the  $m+1^{\text{th}}$  time step is then as follows:

$$\psi_D^{(m+1)} = \frac{1 - iH_{eff}^{(m)}\frac{\Delta t}{2}}{1 + iH_{eff}^{(m)}\frac{\Delta t}{2}}\psi_D^{(m)} + S^{(m)} - M^{(m)} \quad (13)$$

where  $H_{eff}^{(m)} = H_D^{(m)} - \sum_{\alpha} i\frac{\Delta t}{2}H_{C\alpha}(1 + \frac{\Delta t}{2}H_{\alpha\alpha})^{-1}H_{\alpha D}$  is the effective Hamiltonian for the device region, with  $H^{(m)} = \frac{1}{2}[H(t_{m+1}) + H(t_m)]$ . The source term  $S^{(m)}$  corresponds to second last term in equation while the memory term  $M^{(m)}$  corresponds to the last term. The above equation is accurate up to second order and is norm-conserving, which means that it is not necessary to normalize the wavefunction at each time step. With proper transparent boundary condition, the above equation can be propagated to obtain time-dependent Kohn-Sham wavefunction for device region.

There are many works in combining TDDFT and NEGF formalism afterwards. In 2007, Chen et al. prove the HEDT for time-dependent system, thus validate the idea of extending TDDFT formalism to open system.<sup>24</sup> They proposed two approximated numerical schemes, the second order approximation and the adiabatic wide-band limit (AWBL) approximation, to simulate the transient current through some more realistic molecular devices such as a graphene-alkene-graphene system. Under the AWBL approximation, the self-energy is assumed to be independent of energy. In this case, the energy structures of the leads are ignored. There are also other schemes which include, for instance, solving directly the double time-integral Dyson equation,<sup>26</sup> solving the Kadanoff-Baym equations<sup>48-51</sup> and the Kohn-Sham Master Equation approach.<sup>23,52</sup>

It is worth mentioning that solving the time-dependent transport problem without approximation on energy structure of leads, such as the WBL approximation, is a difficult and very computationally expensive task. The major difficulty lies in the memory term. It involves a time integral of the past history from initial time  $t_0$  to the current time step  $t$ , which is unavoidable whichever scheme you choose and this makes the computational cost scale super-linearly with the total simulation time. In fact, a simple implementation will result in computational cost scaling as  $O(t_s^3)$ , where  $t_s$  is the total simulation time.

In an attempt to reduce the computational complexity with respect to the simulation time, Wang et al. developed a method to reduce the complexity from  $O(t_s^3)$  to  $O(t_s^2 \log^2(t_s))$ .<sup>50</sup> To achieve this, they have to avoid solving Poisson equation at each time step self-consistently from the electron density for the coulomb potential and assume that the coulomb potential immediately reaches the steady state value after switching on the step-like bias voltage. Then they employ fast Fourier transform (FFT) techniques in propagating the Kadanoff-Baym equation for the retarded device Green's function, achieving an  $O(t_s^2 \log^2(t_s))$  scaling.

In the following section, we will focus on a particular approach: the reduced single electron density matrix (RSDM) based hierarchical equation of motion (HEOM) approach, **which is able to achieve linear scaling over simulation time. And some numerical results of TDDFT simulation of quantum transport in molecular devices will be reviewed.**

## V. REDUCED SINGLE ELECTRON DENSITY MATRIX BASED HIERARCHICAL EQUATION OF MOTION APPROACH

The RSDM based HEOM approach originates from the Liouville-von Neumann equation.<sup>25</sup> In this approach, the basic variable is the RSDM instead of the Kohn-Sham orbitals. The Liouville-von Neumann equation for the device region with the electronic degrees of freedom of the electrodes projected out is known as:

$$i \frac{d}{dt} \sigma_D(t) = [h_D, \sigma_D] - i \sum_{\alpha} Q_{\alpha}(t) \quad (14)$$

Where  $\sigma_D(t)$  is the RSDM for device region and is equivalent to the lesser Green's function at  $t = t'$  [ $\sigma_D(t) = -iG_D^<(t, t)$ ] in NEGF language.  $Q_{\alpha}(t) = i[h_{D\alpha}\sigma_{\alpha D} - \sigma_{D\alpha}h_{\alpha D}]$  is known as the dissipative term between device and lead  $\alpha$ . In NEGF formalism, it can

be expressed as:

$$Q_{\alpha}(t) = \int_{-\infty}^{\infty} d\tau [\Sigma_{\alpha}^r(t, \tau) G_D^<(\tau, t) + \Sigma_{\alpha}^<(t, \tau) G_D^a(\tau, t) + H.c.] \quad (15)$$

The trace of  $Q_{\alpha}(t)$  gives time-dependent electric current passing from lead  $\alpha$  into the device region.

$$J_{\alpha}(t) = -e \frac{d}{dt} \int_{\alpha} d\vec{r} \rho(\vec{r}, t) = -e \text{Tr}[Q_{\alpha}(t)] \quad (16)$$

Given the TD-HEDT, equation (14) is in principle a closed equation of motion for RSDM since the Kohn Sham Hamiltonian  $h_D(t)$  and the dissipative term  $Q_{\alpha}(t)$  are both functionals of electron density  $\sigma_D(t)$  in device region. In practice, instead of evaluating  $Q_{\alpha}(t)$  from its definition and propagate equation (14), a hierarchical equation of motion is derived and propagated instead. The HEOM is known as follows:<sup>25</sup>

$$\begin{aligned} i\dot{\sigma}_D(t) &= [h_D, \sigma_D] - \sum_{\alpha} \int d\varepsilon [\varphi_{\alpha}(\varepsilon, t) - \varphi_{\alpha}^{\dagger}(\varepsilon, t)] \\ i\dot{\varphi}_{\alpha}(\varepsilon, t) &= [h_D(t) - \varepsilon - \Delta_{\alpha}] \varphi_{\alpha}(\varepsilon, t) + [f_{\alpha}(\varepsilon) \\ &\quad - \sigma_D] \Lambda_{\alpha}(\varepsilon) + \sum_{\alpha'} \int d\varepsilon' \varphi_{\alpha, \alpha'}(\varepsilon, \varepsilon', t) \\ i\dot{\varphi}_{\alpha, \alpha'}(\varepsilon, \varepsilon', t) &= [\varepsilon' + \Delta_{\alpha'}(t) - \varepsilon - \Delta_{\alpha}(t)] \varphi_{\alpha, \alpha'}(\varepsilon, \varepsilon', t) \\ &\quad + \Lambda_{\alpha'}(\varepsilon') \varphi_{\alpha}(\varepsilon, t) - \varphi_{\alpha'}^{\dagger}(\varepsilon', t) \Lambda_{\alpha}(\varepsilon) \end{aligned} \quad (17)$$

where  $\varphi_{\alpha}(\varepsilon, t)$  and  $\varphi_{\alpha, \alpha'}(\varepsilon, \varepsilon', t)$  are known as the 1st and 2nd tier auxiliary RSDM defined by:

$$\begin{aligned} \varphi_{\alpha}(\varepsilon, t) &= -i \left[ \int_C d\tau \mathbf{G}_D(t, \tau) \Sigma_{\alpha}(\varepsilon; \tau, t) \right]^< \\ &= i \int_{-\infty}^t d\tau [\mathbf{G}_D^<(t, \tau) \Sigma_{\alpha}^>(\varepsilon; \tau, t) - \mathbf{G}_D^>(t, \tau) \Sigma_{\alpha}^<(\varepsilon; \tau, t)] \\ \varphi_{\alpha, \alpha'}(\varepsilon, \varepsilon', t) &= i \left[ \int_C d\tau_1 \int_C d\tau_2 \Sigma_{\alpha'}(\varepsilon'; t, \tau_1) \mathbf{G}_D(\tau_1, \tau_2) \Sigma_{\alpha}(\varepsilon; \tau_2, t) \right]^< \end{aligned} \quad (18)$$

A comparison with equation 14 gives  $Q_{\alpha}(t)$  in terms of  $\varphi_{\alpha}(\varepsilon, t)$ :

$$Q_{\alpha}(t) = -i \int d\varepsilon [\varphi_{\alpha}(\varepsilon, t) - \varphi_{\alpha}^{\dagger}(\varepsilon, t)] \quad (19)$$

The above HEOM can be derived easily with the help of NEGF formalism, by differentiating the equation (18) and applying the equation of motion for device lesser/greater Green's function  $G_D^{>/<}(t, t')$  and the equation of motion of energy dispersed self-energy

$\Sigma_{\alpha}^{>/<}(\varepsilon, \tau, t)$ :

$$\begin{aligned} i \frac{\partial}{\partial t} \mathbf{G}_D^<(t, t') &= \mathbf{h}_D(t) \mathbf{G}_D^<(t, t') \\ &\quad + \sum_{\alpha} \int_{-\infty}^{\infty} d\tau [\Sigma_{\alpha}^r(t, \tau) \mathbf{G}_D^<(\tau, t') + \Sigma_{\alpha}^<(t, \tau) \mathbf{G}_D^a(\tau, t')] \\ i \frac{\partial}{\partial t} \Sigma_{\alpha}^{<,>}(\varepsilon, t, t') &= [\varepsilon + \Delta_{\alpha}(t)] \Sigma_{\alpha}^{<,>}(\varepsilon, t, t') \end{aligned} \quad (20)$$

It is noted that unlike the HEOM for reduced (many-electron) density matrix, which has infinitely many tiers,<sup>53</sup> the HEOM for reduced single-electron density matrix **within TDDFT scheme** is closed exactly at the 2nd tier. This is a consequence of the non-interacting na-

ture of Kohn-Sham reference system in TDDFT formalism. The RSDM based HEOM is thus expected to be a computationally efficient and in principle exact approach within the TDDFT-NEGF formalism.

### A. Numerical implementation

In practical implementation, we have to find ways to evaluate energy-integral in the HEOM, which means to convert the integral into a summation. Two decomposition schemes have been proposed and applied to tight-binding model calculation. The Chebyshev decomposition scheme<sup>54</sup> is an accurate scheme and is applicable to **both finite and zero temperature**, though it can be computationally expensive since the number of expansion terms is directly proportional to the simulation time. On the other hand, the Lorentzian-Padé decomposition scheme<sup>55</sup> is an approximated scheme beyond WBL approximation. It involves approximating the linewidth function  $\Lambda_\alpha(E) = i[\Sigma_\alpha^r(E) - \Sigma_\alpha^a(E)]$  by a summation of Lorentzian functions and decompose the Fermi-Dirac distribution by Padé spectrum decomposition:<sup>56</sup>

$$\Lambda_\alpha(\epsilon) \approx \sum_{d=1}^{N_d} \frac{w_d^2}{(\epsilon - \Omega_d)^2 + w_d^2} \bar{\Lambda}_{\alpha,d}, \quad (21)$$

$$f(\epsilon - \mu) \approx \frac{1}{2} - \sum_p \left( \frac{R_p}{\epsilon - \mu + iz_p} + \frac{R_p}{\epsilon - \mu - iz_p} \right). \quad (22)$$

In this case, the lesser self-energy in time domain can be evaluated analytically by Cauchy's residue theorem.

$$\begin{aligned} \Sigma_\alpha^{<, >}(t, t') &= \frac{i}{2\pi} \int_{-\infty}^{\infty} d\epsilon f_\alpha^{<, >}(\epsilon) \Lambda_\alpha(\epsilon) e^{i\epsilon(t'-t)} e^{i \int_t^{t'} d\tau \Delta_\alpha(\tau)} \\ &= \sum_k \mathbf{A}_{\alpha,k}^{<, >} e^{i\epsilon_{\alpha,k}(t'-t)} e^{i \int_t^{t'} d\tau \Delta_\alpha(\tau)} \end{aligned} \quad (23)$$

where  $\epsilon_{\alpha,k}$  are the poles of  $\Lambda_\alpha(\epsilon)$  and  $f_\alpha^{<, >}(\epsilon)$  on the upper half complex plane. For poles of  $\Lambda_\alpha(\epsilon)$ :

$$\epsilon_{\alpha,d} = \Omega_d + iW_d \quad (24)$$

$$\mathbf{A}_{\alpha,d}^{<, >} = \pm i \frac{w_d}{2} \bar{\Lambda}_{\alpha,d} f_\alpha^{<, >}(\epsilon_{\alpha,d} - \mu_\alpha) \quad (25)$$

For poles of  $f_\alpha^{<, >}(\epsilon)$ :

$$\epsilon_{\alpha,p} = \mu_\alpha + iz_p \quad (26)$$

$$\mathbf{A}_{\alpha,p}^{<, >} = R_p \Lambda_\alpha(\epsilon_{\alpha,p}). \quad (27)$$

The energy-resolved self-energy can then be redefined as

$$\Sigma_{\alpha,k}^{<, >}(t, t') = \mathbf{A}_{\alpha,k}^{<, >} e^{i\epsilon_{\alpha,k}(t'-t)} e^{i \int_t^{t'} d\tau \Delta_\alpha(\tau)}. \quad (28)$$

The HEOM under the Lorentzian-Padé decomposition scheme is then as follows,

$$\begin{aligned} i\dot{\boldsymbol{\sigma}}_D(t) &= [\mathbf{h}_D(t), \boldsymbol{\sigma}_D(t)] - \sum_{\alpha,k} (\varphi_{\alpha,k}(t) - \varphi_{\alpha,k}^\dagger(t)) \\ i\dot{\boldsymbol{\varphi}}_{\alpha,k}(t) &= [\mathbf{h}_D(t) - (\epsilon_{\alpha,k} + \Delta_\alpha)] \varphi_{\alpha,k}(t) \\ &\quad - [i\mathbf{A}_{\alpha,k}^< + \boldsymbol{\sigma}_D \Lambda_{\alpha,k}] + \sum_{\alpha'k'} \int \varphi_{\alpha k, \alpha' k'}(t) \\ i\dot{\boldsymbol{\varphi}}_{\alpha k, \alpha' k'}(t) &= [\bar{\epsilon}_{\alpha', k'} + \Delta_{\alpha'}(t) - \epsilon_{\alpha, k} - \Delta_\alpha(t)] \varphi_{\alpha k, \alpha' k'}(t) \\ &\quad + \Lambda_{\alpha', k'} \varphi_{\alpha, k}(t) - \varphi_{\alpha', k}^\dagger(t) \Lambda_{\alpha, k}, \end{aligned} \quad (29)$$

where  $\Lambda_{\alpha,k} = i(\mathbf{A}_{\alpha,k}^> - \mathbf{A}_{\alpha,k}^<)$  and the summation over  $k$  includes all Padé and Lorentzian terms. The major advantage of using the Lorentzian-Padé decomposition scheme is that the computational complexity scales linearly with the simulation time, i.e.  $O(t_s)$ . The number of auxiliary RSDM required depends on the **number of Lorentzian function and Padé decomposition which is determined by** electronic structure of the electrodes as well as the temperature.

### B. Tight-binding model simulation

The Lorentzian-Padé decomposition scheme has been applied to simulate the time-dependent transport through a one dimension nearest neighbour tight-binding chain<sup>55</sup> and study how the device-lead coupling will affect the transport properties. Two cases were studied: **strong and weak device-lead coupling** as illustrated in Fig. 3. The device region consists of two sites and an electronic temperature of 300K is used in the simulation. In the good contact case, the lead-device coupling is set at 1.8eV, slightly less than the coupling inside the device and lead which is 2eV. In the poor contact case, the lead-device coupling is changed to 0.4eV. 4 Lorentzian functions are used to fit the linewidth function  $\Lambda_\alpha(E) = i[\Sigma_\alpha^r(E) - \Sigma_\alpha^a(E)]$  and 10 terms are used in Padé decomposition of Fermi-Dirac distribution. **After the voltage is applied, a linear potential drop in the device region is assumed.**

Fig. 4 shows from left to right the I-V characteristics, the local density of state in the device region and the transient current respectively. The upper row shows the results for the strong contact case while the lower row is for weak contact case.

For the strong contact case, it can be seen that at small voltages, the I-V curve is linear. But when we keep increasing the voltage, the curve bends down. This is known as the negative differential resistance (NDR)<sup>57</sup> and is a important feature in semiconductor devices such as resonant tunneling diode.<sup>7</sup> Here, the NDR is due to the finite band width of leads. The current decreases at large voltage because the energy band of the leads is shifted away from the two energy levels in the device.

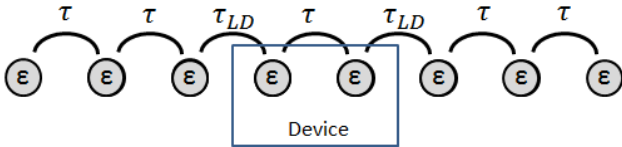


FIG. 3. Nearest neighbour tight-binding model simulated. Good contact:  $\tau = 2.0eV, \tau_{LD} = 1.8eV$ ; Poor contact:  $\tau = 2.0eV, \tau_{LD} = 0.4eV$

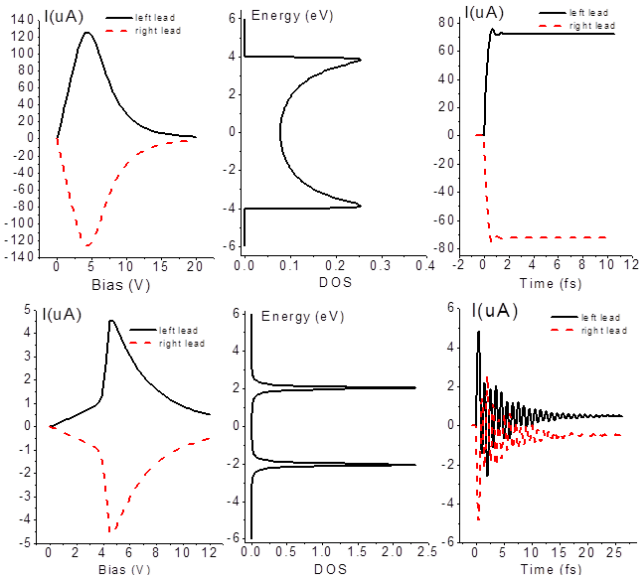


FIG. 4. I-V curve (left), DOS spectrum (middle) and the transient current (right) for a 2-atom device with strong contact (upper row) and weak contact (lower row). The bias voltage is 2V and is switched on suddenly as a step function.

For the transient current, we can see that it reaches the steady state smoothly and rapidly in about 2 femtoseconds(fs).

For the poor contact case, due to the weak coupling to the lead, the linewidth function  $\Lambda_\alpha(E)$  is small and this results in two sharp peaks in the DOS diagram corresponding to the two energy level in device region. The small peak broadening means that the electrons would have a long lifetime inside the device region. In the I-V curve, the current is in general much smaller than that in strong contract case due to the weak coupling. The current shows a sharp increase at 4V because at that point, the chemical potential of the lead is shifted to align with the energy level in the device. This results in resonant tunneling. The transient current shows large and long lasting oscillation before reaching the steady state. The amplitude of the oscillation at the beginning can even be much larger than the steady state current. This long lasting oscillation is again due to the long lifetime of electrons in the device, so they oscillate in device with a small

damping before reaching a steady state.

## VI. WIDE BAND LIMIT APPROXIMATION

### A. RSDM based HEOM in WBL approximation

As mentioned, solving the time-dependent transport problem without approximation is computationally very expensive, especially for first principle simulation of realistic systems. The computational complexity of 2nd-tier HEOM lies in the large number of second tier auxiliary density matrix have to be evaluated. In order to simulate the complex system containing hundreds or thousands of atoms, further approximation should be made to reduce the computational complexity. It is shown that the HEOM terminates at the first tier when WBL approximation is adopted,<sup>25,28</sup> and have been implemented with TDDFT and TD-DFTB method.<sup>28</sup> Under the WBL approximation, it is assumed that the band-widths of the leads are infinitely large (wide band) and the line-widths are energy-independent. i.e.,  $\tilde{\Lambda}_\alpha(\epsilon) = \tilde{\Lambda}_\alpha$  [ $\tilde{\Lambda}_\alpha(\epsilon) = \Lambda_\alpha(\epsilon)/2$ ]. In this case, the energy dependent features of the leads are ignored. The self-energy then becomes

$$\Sigma_\alpha^{<,>}(\tau, t) = \pm 2i\tilde{\Lambda}_\alpha \int \frac{d\epsilon}{2\pi} f_\alpha^{<,>}(\epsilon) e^{i \int_\tau^t [\epsilon + \Delta_\alpha(t_1)] dt_1}, \quad (30)$$

where  $\tilde{\Lambda}_\alpha = \pi \sum_{k_\alpha} |V|^2 \delta(\epsilon_f - \epsilon_{k_\alpha})$  is the line-width function evaluated at the Fermi energy  $\epsilon_f$  of the unbiased system. The Fermi-Dirac distribution function again can be expanded using Padé spectrum decomposition in Eq. (22). For certain system at temperature  $T$ , the number of Padé expansion is chosen such that the validity length  $L$ , defined by  $\delta f(\epsilon)|_{\beta(\epsilon - \mu_\alpha) = L} = \delta$ , where  $\delta$  is the tolerance desired in the simulation, is equal to  $\beta(\epsilon_{max} + |\mu_\alpha|)$ , where  $\epsilon_{max}$  is the maximum absolute value of the eigenvalues of Fock matrix.

With the Padé expansion and WBL approximation, the time-domain lesser self-energy in Eq.(30) can be evaluated analytically through contour integration and Cauchy's residue theorem, which results in:

$$\Sigma_\alpha^{<,>}(\tau, t) \approx \pm \frac{i}{2} \delta(t - \tau) \tilde{\Lambda}_\alpha + x \sum_k^N \Sigma_{\alpha k}^x(\tau, t), \quad (31)$$

where  $x = +$  for  $t \geq \tau$  and  $x = -$  for  $t < \tau$ , corresponding to upper (+) or lower half plane (-) contour integration.  $\Sigma_{\alpha k}^\pm(\tau, t)$  is defined as

$$\Sigma_{\alpha k}^\pm(\tau, t) = 2R_k e^{i \int_\tau^t \tilde{\epsilon}_{\alpha k}^\pm(t_1) dt_1} \tilde{\Lambda}_\alpha, \quad (32)$$

where  $\tilde{\epsilon}_{\alpha k}^\pm(t) = \pm iz_k + \mu_\alpha + \Delta_\alpha(t)$ . The first tier auxiliary density matrix is then evaluated as:

$$\begin{aligned} \varphi_\alpha(t) &= i \int_{-\infty}^t d\tau [\mathbf{G}_D^{<}(t, \tau) \Sigma_\alpha^{>}(\tau, t) - \mathbf{G}_D^{>}(t, \tau) \Sigma_\alpha^{<}(\tau, t)] \\ &= i[\sigma(t) - 1/2] \Lambda_\alpha + \sum_k^N \varphi_{\alpha k}(t). \end{aligned} \quad (33)$$

The first term on the right hand side (RHS) comes from the integration over  $G_D^{>/<}(t, \tau)$  and delta function  $\delta(\tau - t)$ . The energy-discretized first tier ARSDMs  $\varphi_{\alpha k}(t)$  are defined as:

$$\varphi_{\alpha k}(t) = -i \int_{-\infty}^{\infty} d\tau G^r(t, \tau) \Sigma_{\alpha k}^+(\tau, t), \quad (34)$$

And each of them evolves according to the following EOM, which can be derived easily since the EOMs of  $G^r(t, \tau)$  and  $\Sigma_{\alpha k}^+(\tau, t)$  are simply linear equations of themselves.

$$i\dot{\varphi}_{\alpha k}(t) = -2iR_k\tilde{\Lambda}_\alpha - [\tilde{\epsilon}_{\alpha k}^+(t) - h(t) + i\tilde{\Lambda}] \varphi_{\alpha k}(t), \quad (35)$$

where  $\tilde{\Lambda} = \sum_\alpha \tilde{\Lambda}_\alpha$  is the total line-width function of two leads.

Under the WBL approximation, Eqs.(14), (33) and (35) give us a close set of EOMs, without the need to introduce the second tier auxiliary density matrices, which is termed as the NEGF-HEOM-WBL method. Thus propagating this set of EOMs with proper initial values gives the time-dependent density matrix, auxiliary density matrices and calculate the time-dependent quantities of interest from them. Since no second tier auxiliary density matrices are required, the WBL approximation is therefore much more desirable in terms of computational time as well as memory requirement for simulating large realistic devices.

For the initial values for the EOMs, at initial time  $t = 0$  before switching on the bias voltage, the whole system should be in equilibrium. All quantities are therefore time-independent, so do the RSDM and ARSDMs. By requiring Eqs. (14) and (35) to equal to zero at initial time, the initial conditions are given by:

$$\sigma(0) = \frac{1}{2}\mathbf{I} + \sum_{\alpha k} \text{Re} \left( \frac{2R_k}{\tilde{\epsilon}_{\alpha k}(0) - h(0) + i\tilde{\Lambda}} \right). \quad (36)$$

$$\varphi_{\alpha k}(0) = -\frac{2iR_k}{\tilde{\epsilon}_{\alpha k}(0) - h(0) + i\tilde{\Lambda}} \tilde{\Lambda}_\alpha. \quad (37)$$

These two equations provide the initial conditions for the EOMs. After bias voltage is switched on, the device is driven out of equilibrium and the dynamic response of the device can be obtained by solving the EOMs of  $\sigma(t)$  and  $\varphi_{\alpha k}(t)$  in time domain.

## B. TDDFT(B)-NEGF-HEOM-WBL formalism

This NEGF-HEOM-WBL formalism has been implemented in the framework of TDDFT and time-dependent density functional tight-binding (TDDFTB) method, which is called TDDFT(B)-NEGF-HEOM-WBL formalism.<sup>28</sup> In this formalism, the system is assumed to be in its ground state initially, which is determined by molecular cluster based technique.<sup>24</sup> In the

ground state calculation, not only the device region but also a portion of the leads have to be included in the extended cluster so that the the periodic diagonal and off-diagonal blocks of lead KS Hamiltonian  $h_{LL/RR}$  is extracted from the whole KS Hamiltonian to evaluate the surface Green's function  $g_{L/R}$ <sup>58</sup> and extract the device-lead coupling matrix  $h_{DL/DR}$  to calculate line-width function  $\Lambda_{L/R}$ . The initial values for  $\sigma_D$  and  $\varphi_{\alpha k}$  are then evaluated as described above.

The time propagation of the density matrix  $\sigma(t)$  and auxiliary density matrix  $\varphi_{\alpha k}(t)$  was carried out with the fourth-order Runge-Kutta (RK4) method. After bias voltage is turned on, The KS Fock matrix changes with time according to the induced electron density. The change in KS Fock matrix comprises of two parts, the induced Hartree potential  $V_H(\mathbf{r}, t)$  and induced XC potential  $V_{xc}(\mathbf{r}, t)$ .

$$h(t) = h(0) + \delta V_H(t) + \delta V_{xc}(t), \quad (38)$$

where  $h(0)$  is the ground state KS Fock matrix. These two components  $\delta V_H(t)$  and  $\delta V_{xc}(t)$  have to be updated at each time step according to the induced electron density  $\delta n(\mathbf{r}, t)$ , which is a consequence of the voltage applied at the leads.

To obtain them, the induced Hartree and XC potential are first solved in real space followed by projecting them on the basis set. The evaluation of induced XC potential depends on which XC functional we employ and the induced Hartree potential is obtained by solving the Poisson equation:

$$\nabla^2 \delta V_H(\mathbf{r}, t) = -4\pi \delta n(\mathbf{r}, t), \quad (39)$$

subject to the boundary condition at the lead-device interface:

$$\begin{aligned} \delta V_H(\mathbf{r}, t)|_{S_L} &= V_L(t), \\ \delta V_H(\mathbf{r}, t)|_{S_R} &= V_R(t), \end{aligned} \quad (40)$$

where  $S_L/S_R$  are the the interfaces between device and leads;  $V_{L/R}(t)$  is the bias voltage applied on lead  $L/R$ .

Transient current at each time step is obtained from Eq.(16). The most time-consuming part is the propagation of the first tier ARSDMs  $\varphi_{\alpha k}$ , since there are  $2N_k$   $\varphi_{\alpha k}(t)$  matrices to be propagated at each time step. To reduce the computational cost, the sparsity of the line-width function  $\Lambda_\alpha$ , which is localized on the top left or bottom right corner, was taken into account and only a small block of  $\Lambda_\alpha$  and a partial block of  $\varphi_{\alpha k}(t)$  were calculated in the numerical implementation. As a result, the computational cost and memory requirement are reduced and simulating large systems is possible with this method.

## C. First principle simulation results

The above TDDFT(B)-NEGF-HEOM-WBL method has been applied to simulate in first principle the ac response of a (5, 5) carbon nanotube(CNT)-based device.<sup>28</sup>

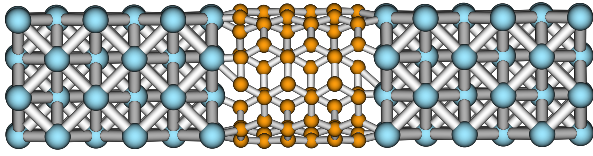


FIG. 5. CNT-based device. There are 60 atoms for the (5, 5) CNT and 16 atoms in a unit cell of aluminum leads.

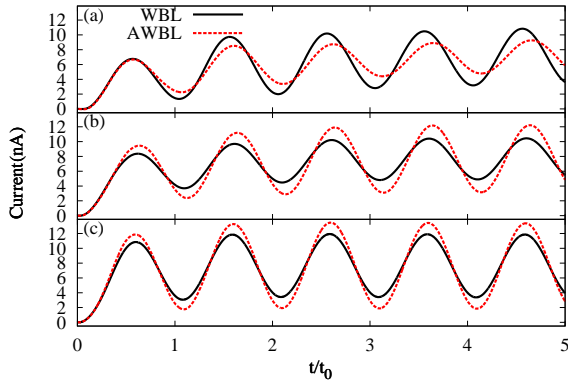


FIG. 6. TDDFT calculation of transient current corresponding to sinusoidal bias voltage,  $V(t) = \frac{V_0}{2}[1 - \cos(\frac{2\pi t}{t_0})]$ ,  $V_0 = 0.1\text{meV}$ . (a)  $t_0 = 2\text{fs}$ ; (b)  $t_0 = 5\text{fs}$ ; (c)  $t_0 = 10\text{fs}$ . The black real line is WBL current; Red dash line is AWBL current.

As shown in Fig. 5, it comprises of a (5, 5) CNT, which contains 60 carbon atoms, connected to two aluminum leads from left and right. The distance between the CNT and the aluminum lead is  $1.5\text{\AA}$ . The device region includes the CNT as well as one unit cell of the aluminum lead on each side. The whole device region thus contains 60 carbon atoms and 32 aluminum atoms.

Simulations were done in both TDDFT and TDDFTB levels as shown in Fig. 6 and 7 respectively. Comparison with the AWBL approximation (Ref. 24) is made. Since the AWBL method is applicable for zero-temperature while the WBL scheme here is not, the WBL simulation is carried out at very low temperatures (5K in this case) so as to make the comparison meaningful.

The core orbitals are excluded through a projector operator<sup>59</sup> since the core orbitals will play little role in quantum transport. The largest absolute value of the eigenvalues of Fock matrix is found to be around 19eV after excluding core orbitals. A 300 terms Padé expansion is used for the WBL simulation to achieve tolerance  $\delta = 10^{-7}$  for a validity length equal to  $4.4 \times 10^4$ . RK4 propagation with time step equal to 0.015fs is used. In TDDFT simulation, the minimal basis set STO-3G is employed and the adiabatic localized density approximation (ALDA) is chosen as the XC functional.

Given the alternating bias voltage, the system is always driven out of steady state. Therefore, the memory effect here plays a more important role than that for exponential growth bias voltage. It can be seen that

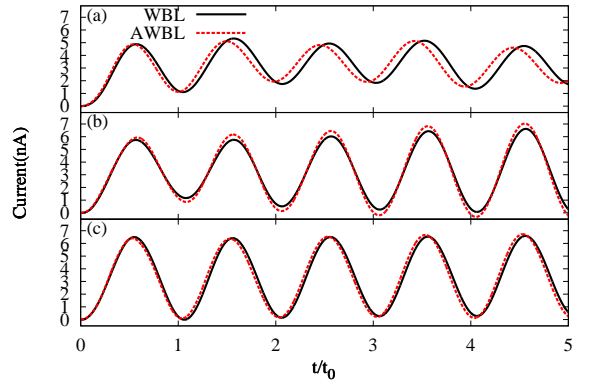


FIG. 7. TDDFTB simulation of transient current corresponding to sinusoidal bias voltage,  $V(t) = \frac{V_0}{2}[1 - \cos(\frac{2\pi t}{t_0})]$ ,  $V_0 = 0.1\text{meV}$ . (a)  $t_0 = 2\text{fs}$ ; (b)  $t_0 = 5\text{fs}$ ; (c)  $t_0 = 10\text{fs}$ . The black real line is WBL current; Red dash line is AWBL current.

for both TDDFT and TDDFTB simulations, the AWBL and WBL results agree well with each other under low frequency ac voltage but give different amplitude and phase delays under high frequency bias. This is especially obvious in the case of TDDFTB simulation under the high frequency bias ( $t_0 = 2\text{fs}$ ), in which the AWBL current even leads before the bias voltage. It is thus concluded that the WBL method is more suitable for high frequency simulations whereas the AWBL is good enough for simulations at low frequency.

## VII. CONCLUDING REMARKS

First-principles method for the quantum transport has seen tremendous growth of research interest, however the majority of studies focus on the steady state properties. Besides, the DFT-NEGF method for quantum transport has its theoretical weakness as DFT is a ground state theory and therefore not suitable for non-equilibrium phenomena. Based on the TD-HEDT, the existence of rigorous first-principles method for quantum transport is confirmed. Consequently, an exact formula was developed in terms of HEOM for RSDM and auxiliary density matrices followed by several practical numerical scheme at different levels of approximation as reviewed in this manuscript.

Even through the foundation of TDDFT for quantum transport have been laid, this field is at an early stage in its development, there are still plenty of rooms for further development and applications. Firstly, the accuracy of TDDFT method for quantum transport is limited by the quality of exchange-correlation functional. The exchange-correlation effect between electrons is intimately related to the quantum transport phenomena. For instance, the discontinuity of exchange-correlation potential of TDDFT is crucial for the description of

coulomb blockade.<sup>60</sup> More efforts have to be paid to the development of exchange-correlation functionals for the quantum transport problems. Secondly, previous studies in the TDDFT for quantum transport did not consider the dissipation due to electron-phonon scattering. The inelastic effect due to electron-phonon scattering can play a vital role in the functionality and stability of current-carrying devices. Thus future work of TDDFT for quantum transport should take into account the dissipation due to electron-phonon interaction.

## ACKNOWLEDGMENTS

Support from the Hong Kong Research Grant Council (Contract Nos. HKU7009/09P, 7008/08P, 7007/11P, and HKUST 9/CRF/08), and the University Grant Council (Contract No. AoE/P-04/08) is gratefully acknowledged.

\* ghc@everest.hku.hk

- <sup>1</sup> M. Auf der Maur, M. Povolotskiy, F. Sacconi, A. Pecchia, G. Romano, G. Penazzi, and A. Di Carlo, *Opt. Quantum Electron* **40**, 1077 (2008).
- <sup>2</sup> M. C. Petty, *Molecular Electronics: From Principles to Practice* (Wiley, 2008) p. 544.
- <sup>3</sup> A. Aviram and M. A. Ratner, *Chem. Phys. Lett* **29**, 277 (1974).
- <sup>4</sup> M. A. Reed, C. Zhou, C. J. Muller, T. P. Burgin, and J. M. Tour, *Science* **278**, 252 (1997).
- <sup>5</sup> H. Song, Y. Kim, Y. H. Jang, H. Jeong, M. A. Reed, and T. Lee, *Nature* **462**, 1039 (2009).
- <sup>6</sup> H. Song, M. A. Reed, and T. Lee, *Advanced Materials* **23**, 1583 (2011).
- <sup>7</sup> S. W. Wu, N. Ogawa, and W. Ho, *Science* **312**, 1362 (2006).
- <sup>8</sup> M. Galperin and A. Nitzan, *Phys. Chem. Chem. Phys.* **14**, 9421 (2012).
- <sup>9</sup> A. Nitzan and M. A. Ratner, *Science* **300**, 1384 (2003).
- <sup>10</sup> M. Paulsson, T. Frederiksen, and M. Brandbyge, *Nano Letters* **6**, 258 (2006).
- <sup>11</sup> G. Michael and et al., *J. Phys.: Condensed Matter* **19**, 103201 (2007).
- <sup>12</sup> J. C. Cuevas and E. Scheer, *Molecular Electronics: An Introduction to Theory and Experiment*, Vol. 1 (World Scientific Series in Nanotechnology and Nanoscience, 2010) p. 703.
- <sup>13</sup> T. Fujisawa, D. G. Austing, Y. Tokura, Y. Hirayama, and S. Tarucha, *J. Phys.: Condens. Matter* **15** (2003).
- <sup>14</sup> J. Taylor, H. Guo, and J. Wang, *Phys. Rev. B* **63**, 245407 (2001).
- <sup>15</sup> M. Brandbyge, J.-L. Mozos, P. Ordejón, J. Taylor, and K. Stokbro, *Phys. Rev. B* **65**, 165401 (2002).
- <sup>16</sup> M. Elstner, D. Porezag, G. Jungnickel, J. Elsner, M. Haugk, T. Frauenheim, S. Suhai, and G. Seifert, *Phys. Rev. B* **58**, 7260 (1998).
- <sup>17</sup> T. A. Niehaus, S. Suhai, F. Della Sala, P. Lugli, M. Elstner, G. Seifert, and T. Frauenheim, *Phys. Rev. B* **63**, 085108 (2001).
- <sup>18</sup> C. Yam, L. Meng, G. Chen, Q. Chen, and N. Wong, *Phys. Chem. Chem. Phys.* **13**, 14365 (2011).
- <sup>19</sup> L. Meng, C. Yam, S. Koo, Q. Chen, N. Wong, and G. Chen, *Journal of Chemical Theory and Computation* **8**, 1190 (2012).
- <sup>20</sup> G. Stefanucci and C. O. Almbladh, *EPL (Europhysics Letters)* **67**, 14 (2004).
- <sup>21</sup> J. Maciejko, J. Wang, and H. Guo, *Phys. Rev. B* **74**, 085324 (2006).
- <sup>22</sup> S. Kurth, G. Stefanucci, C.-O. Almbladh, A. Rubio, and E. K. U. Gross, *Phys. Rev. B* **72**, 035308 (2005).
- <sup>23</sup> J. Yuen-Zhou, D. G. Tempel, C. A. Rodríguez-Rosario, and A. Aspuru-Guzik, *Phys. Rev. Lett.* **104**, 043001 (2010).
- <sup>24</sup> X. Zheng, F. Wang, C. Y. Yam, Y. Mo, and G. Chen, *Phys. Rev. B* **75**, 195127 (2007).
- <sup>25</sup> X. Zheng, G. Chen, Y. Mo, S. Koo, H. Tian, C. Yam, and Y. Yan, *J. Chem. Phys.* **133**, 114101 (2010).
- <sup>26</sup> S.-H. Ke, R. Liu, W. Yang, and H. U. Baranger, *The Journal of Chemical Physics* **132**, 234105 (2010).
- <sup>27</sup> K. Burke, R. Car, and R. Gebauer, *Phys. Rev. Lett.* **94**, 146803 (2005).
- <sup>28</sup> Y. Zhang, S. Chen, and G. Chen, *Phys. Rev. B* **87**, 085110 (2013).
- <sup>29</sup> S. Chen, H. Xie, Y. Zhang, X. Cui, and G. Chen, *Nanoscale* **5**, 169 (2013).
- <sup>30</sup> A.-P. Jauho, N. S. Wingreen, and Y. Meir, *Phys. Rev. B* **50**, 5528 (1994).
- <sup>31</sup> Y. ChiYung and et al., *Nanotechnology* **19**, 495203 (2008).
- <sup>32</sup> K. F. Albrecht, H. Wang, L. Mühlbacher, M. Thoss, and A. Komnik, *Phys. Rev. B* **86**, 081412 (2012).
- <sup>33</sup> E. Khosravi, S. Kurth, G. Stefanucci, and E. Gross, *Applied Physics A* **93**, 355 (2008).
- <sup>34</sup> E. Khosravi, G. Stefanucci, S. Kurth, and E. Gross, *Phys. Chem. Chem. Phys.* **11**, 4535 (2009).
- <sup>35</sup> B. Popescu, P. B. Woiczikowski, M. Elstner, and U. Kleinekathöfer, *Phys. Rev. Lett.* **109**, 176802 (2012).
- <sup>36</sup> J. K. Tomfohr and O. F. Sankey, *phys. status solidi (b)* **226**, 115 (2001).
- <sup>37</sup> N. Bushong, N. Sai, and M. Di Ventra, *Nano Letters* **5**, 2569 (2005).
- <sup>38</sup> J. Muga, J. Palao, B. Navarro, and I. Egusquiza, *Physics Reports* **395**, 357 (2004).
- <sup>39</sup> R. Baer, T. Seideman, S. Ilani, and D. Neuhauser, *The Journal of Chemical Physics* **120**, 3387 (2004).
- <sup>40</sup> K. W. Hohenberg P, *Phys. Rev. B* **136**, 864 (1964).
- <sup>41</sup> E. Runge and E. K. U. Gross, *Phys. Rev. Lett.* **52**, 997 (1984).
- <sup>42</sup> S. Fournais, M. Hoffmann-Ostenhof, T. Hoffmann-Ostenhof, and T. Østergaard Sørensen, *Arkiv för Matematik* **42**, 87 (2004).
- <sup>43</sup> S. Fournais, M. Hoffmann-Ostenhof, T. Hoffmann-Ostenhof, and T. Østergaard Sørensen, *Communications in Mathematical Physics* **228**, 401 (2002).
- <sup>44</sup> X. Zheng, C. Yam, F. Wang, and G. Chen, *Phys. Chem. Chem. Phys.* **13**, 14358 (2011).
- <sup>45</sup> G. Vignale and W. Kohn, *Phys. Rev. Lett.* **77**, 2037 (1996).
- <sup>46</sup> M. Di Ventra and R. D'Agosta, *Phys. Rev. Lett.* **98**, 226403 (2007).

- <sup>47</sup> R. D'Agosta and M. Di Ventra, *Phys. Rev. B* **78**, 165105 (2008).
- <sup>48</sup> M. Galperin and S. Tretiak, *The Journal of Chemical Physics* **128**, 124705 (2008).
- <sup>49</sup> Y. Xing, B. Wang, and J. Wang, *Phys. Rev. B* **82**, 205112 (2010).
- <sup>50</sup> L. Zhang, Y. Xing, and J. Wang, *Phys. Rev. B* **86**, 155438 (2012).
- <sup>51</sup> P. Myöhänen, A. Stan, G. Stefanucci, and R. van Leeuwen, *Phys. Rev. B* **80**, 115107 (2009).
- <sup>52</sup> R. Gebauer, K. Burke, and R. Car, in *Time-Dependent Density Functional Theory*, Lecture Notes in Physics, Vol. 706, edited by M. Marques, C. Ullrich, F. Nogueira, A. Rubio, K. Burke, and E. U. Gross (Springer Berlin Heidelberg, 2006) pp. 463–477.
- <sup>53</sup> J. Jin, X. Zheng, and Y. Yan, *J. Chem. Phys.* **128**, 234703 (2008).
- <sup>54</sup> H. Tian and G. Chen, *The Journal of Chemical Physics* **137**, 204114 (2012).
- <sup>55</sup> H. Xie, F. Jiang, H. Tian, X. Zheng, Y. Kwok, S. Chen, C. Yam, Y. Yan, and G. Chen, *J. Chem. Phys.* **137**, 044113 (2012).
- <sup>56</sup> J. Hu, R.-X. Xu, and Y. Yan, *J. Chem. Phys.* **133**, 101106 (2010).
- <sup>57</sup> J. R. Soderstrom, D. H. Chow, and T. C. McGill, *Applied Physics Letters* **55**, 1094 (1989).
- <sup>58</sup> M. P. L. Sancho, J. M. L. Sancho, J. M. L. Sancho, and J. Rubio, *J. Phys. F: Metal Physics* **15**, 851 (1985).
- <sup>59</sup> F. Wang, C. Y. Yam, G. Chen, and K. Fan, *J. Chem. Phys.* **126**, 134104 (2007).
- <sup>60</sup> S. Kurth, G. Stefanucci, E. Khosravi, C. Verdozzi, and E. K. U. Gross, *Phys. Rev. Lett.* **104**, 236801 (2010).